Multi-objective sizing and dispatch for building thermal and battery storage towards economic and environmental synergy☆

Min Gyung Yu *, Bowen Huang, Xu Ma, Karthik Devaprasad

Pacific Northwest National Laboratory, Richland, 99352, WA, USA

ARTICLE INFO

Keywords:
Multi-objective optimization
Optimal sizing
Optimal dispatch
Building energy storage systems

ABSTRACT

The role of building thermal and battery storage is pivotal in advancing smart cities and achieving sustainability goals through effective energy management. Despite their significance, there are several limitations in the sizing approach and value stream analysis with various objectives for their widespread adoption in buildings. This work proposes a flexible and scalable multi-objective optimization framework for optimal sizing and dispatch of building thermal and battery storage, addressing multiple objectives simultaneously using mixed-integer linear programming. The weighted-sum method is adapted, combining multiple objectives into a single function. The two-stage procedure iterates over different weights, generates optimal solutions, and forms the Pareto front. Case studies are performed to assess the energy, economic, and environmental benefits of building energy storage systems for a large office building in three climate locations. The results demonstrate that the proposed framework efficiently determines optimal sizing and dispatch strategies, addressing the balance between economic viability and emission reduction. The dynamic relationship between time-of-use energy charges and emission factors leads to diverse strategies based on whether economic or environmental concerns are prioritized. This research enhances our understanding of the benefits of thermal and battery storage systems in buildings, providing valuable guidance to stakeholders.

1. Introduction

Thermal and battery storage play important roles in the development of smart cities, to contribute to sustainability goals by effectively managing energy resources. Thermal storage systems store thermal energy and release it when required for heating or cooling in buildings. Similarly, battery systems charge electrical energy and discharge it when needed. As strategically harnessing energy resources, this proactive approach helps to balance between energy supply and demand. Its peak load management can reduce the need for fossil fuel power plants during peak demand, and it can enhance the overall utilization of clean energy sources with the nature of energy storage.

Moreover, end-users can further save operational costs by leveraging time-of-use (TOU) rates to get economic benefits with the energy storage [1]. TOU rate tariffs encourage customers to reduce their energy consumption during peak hours when electricity costs are higher and increase consumption during off-peak hours when rates are lower. In addition, building energy storage can utilize more direct resources to lower emissions for a cleaner and more sustainable environment. These days, many resources provide data to quantify the locational carbon intensity to be more carbon-aware and potentially reduce the emission [2,3]. In each region, the emission factor varies due to the sources of the electricity generation, which plays a significant role in determining carbon intensity. For instance, regions with a higher generation of renewable energy sources can have lower emission factors compared to those relying heavily on fossil fuels [2,4]. The marginal emission rates also vary over the time of day due to several factors, including intermittent renewable resources, operational characteristics of power plants, energy demand, and more. Thus, it becomes evident that the operation of thermal and battery storage can provide more environmental benefits.

However, there are several barriers preventing the widespread adoption of thermal and battery storage in buildings. First, the current approach to sizing the storage systems lacks consideration of operational efficiency. The sizing strategies for thermal storage (e.g., full storage operation, partial storage operation) are recommended based on the peak day load profile, however, this would require a larger

☆ This research was supported by the Energy Mission Seed Investment, under the Laboratory Directed Research and Development Program at Pacific Northwest National Laboratory (PNNL). PNNL is a multi-program national laboratory operated for the U.S. Department of Energy by Battelle Memorial Institute under Contract No. DE-AC05-76RL01830.

* Corresponding author.
E-mail address: mingyung.yu@pnnl.gov (M.G. Yu).

plant system [5]. Without energy storage systems in buildings, the capacities of the building plant system are often determined based on the design day and peak demand, which may result in oversized systems that mostly run inefficiently at lower part load ratios [6]. Furthermore, capital costs and physical constraints are often neglected when addressing the optimal sizes. Optimal sizing considering operation and space constraints can lead to economical system sizes and improved efficiency compared to conventional sizing methods. Second, value stream analysis with various objectives has not been addressed. There can be multiple purposes for using thermal and battery storage in buildings. While it is widely known that storage systems are economically advantageous due to their own characteristics, particularly in utilizing the TOU rates to contribute to peak demand reduction [1,7], research focusing on minimizing carbon emissions is still insufficient.

To address these issues, many researchers focused on developing sizing methods for thermal and battery storage in buildings [8–14]. The optimal design of thermal storage has been explored with the operation of the HVAC systems to consider related system-level operation characteristics and efficiency [15,16]. For instance, the charge and discharge strategy of chilled water thermal storage has been studied with chiller dispatch and load conditions [8]. As the problem includes non-linear system behaviors, heuristic algorithms have been proposed; particle swarm optimization (PSO) and genetic algorithm (GA) have been widely used in the optimization framework [9,10,15–17]. A simulation-based optimization framework using PSO has been developed to maximize the energy benefits of the water storage system coupled with a chiller while considering investment and operational costs [16]. The PSO algorithm has also been leveraged to address the optimal sizing and dispatch problem for both thermal and battery storage coupled with renewable energy resources in a residential building [17]. In the meantime, a GA-based optimal design of thermal storage has been proposed to reduce life cycle costs [9]. Moreover, a comprehensive study comparing the performance of five metaheuristic algorithms for optimizing the operating schedule of energy systems with battery and thermal energy storage systems, as well as an air-source heat pump has been conducted [15]. From previous studies, the methods using heuristic algorithms have been validated to provide near-optimal solutions for efficient energy utilization and cost-saving with building thermal storage [10].

The optimal energy and power capacity of battery storage in buildings have been studied using mathematical optimization algorithms [12–14,18]. Linear programming has been leveraged for the optimized battery size to provide economical benefits considering the battery cost and operational costs [12]. The economic benefits and optimal sizes have been analyzed in various regions with different utility rate structures. In addition, the battery size has been studied when integrated with renewable energy resources in residential buildings for nearly zero-energy buildings [13]. The lifespan of the energy assets and capital costs have been considered to minimize the life cycle costs by using the storage to show the life-long efficacy. Another research considered environmental impacts when sizing the battery for zero energy buildings [14,18]. This research considered the environmental impact index indicating climate change and emissions to limit the battery operation in the sizing problem. The problem is solved using mixed-integer linear programming.

While most research on the optimal sizing of batteries used mathematical algorithms to solve the problem, many previous works on thermal storage sizing heavily relied on the heuristic algorithm. Even though the heuristic algorithm can provide nearly optimal solutions, it has limitations in finding the global optimum solution for complex and nonlinear problems. Mathematical optimization algorithms can handle large and complex systems more efficiently and can provide guaranteed optimal solutions. Mathematical optimization algorithms also allow for sensitivity analysis, which helps in understanding the impact of changes in the problem's parameters on the solution. While heuristics can also be used for sensitivity analysis, mathematical optimization algorithms often provide more structured and theoretically grounded methods for conducting such analyses. Some prior studies formulated mixed-integer linear programming and quadratic programming to address the optimal dispatch problem of building thermal storage [19,20] and explored the flexibility potential; however, optimal sizing was not investigated in these works.

In addition to the existing research that focused on the single objective approaches for peak load management and cost saving in sizing and dispatch problems, there is a need for a more comprehensive understanding of value streams with multiple objectives. The optimal size of building thermal and battery storage is a challenging task due to the conflicting nature of the objectives. For instance, building energy storage with large capacity would increase the energy and economic benefits. However, it would lead to unrealistic capital costs. Moreover, significant energy consumption during the charging operation can lead to substantial emissions. Thus, the multi-objective methods have been introduced to design and operate the thermal and battery storage in buildings to concurrently achieve various objectives [21–24]. One research studied the best trade-off between heating and cooling performances when designing thermal storage [21]. Beyond addressing different technical objectives, both economic and technical objectives are considered when integrating the energy storage operation strategy with renewable energy resources [22]. In that regard, previous researchers considered the TOU rates as well as the utilization of renewable energy in the objective functions. This optimization problem was addressed through a GA to obtain the optimal capacity. The GA was also leveraged in the development of thermal and battery storage systems within the building community [23,24]. This problem simultaneously considered economic and emission objectives to minimize both life cycle costs and greenhouse gas emission costs [23].

Even though previous research demonstrated the merit of integrating multiple objectives into the decision-making process, it is essential to note that there are limitations in these approaches relying on heuristic algorithms, as mentioned above. Furthermore, even though emissions were considered in the objectives, the previous studies applied constant emission coefficients for power usage, which does not account for the time-varying nature of emission factors throughout the day. Given the variations in electricity rates and emission factors across regions and during times of the day, more comprehensive research is imperative to maximize the economic and emission benefits of thermal and battery storage. This will provide stakeholders with substantial information to accelerate the large-scale adoption of these building energy storage systems.

Overall, the main limitations in previous research include reliance on heuristic algorithms, which make it difficult to create a flexible framework and perform sensitivity study. Additionally, the multi-objective function needs to consider both varying electricity prices and emission factors throughout the day to fully capture the benefits of using thermal and battery storage.

To bridge these gaps, our work proposes a novel framework that takes into account both thermal and battery storage in buildings, utilizing mixed integer linear programming. Our approach considers the impact of the power market, which has different TOU pricing and demand charge pricing in various regions, for a more realistic and practical solution. We also incorporate the time-varying marginal emission factor to enhance the sophistication of our emission reduction solution.

The key contributions of this article are:

1. A multi-objective optimization based on mixed integer linear programming for optimal sizing and dispatch of building thermal and battery storage to consider multiple objectives (i.e., economic and environmental concerns) and provide a balanced understanding of value streams for better decision-making. Both varying electricity prices and emission factors throughout the day are considered to not only save the customer's electricity bills but also consider using electricity during lower emission periods.

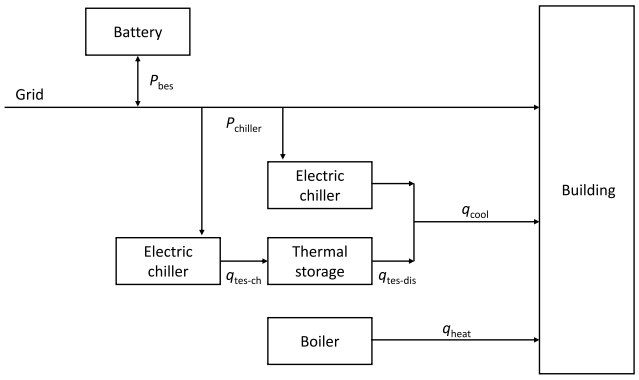

Fig. 1. Energy flow of building energy systems with thermal storage and battery.

2. Adapting a weighted-sum method, multiple objectives are combined into a single function and the Pareto front solutions are generated, allowing stakeholders to choose the final solution based on their priorities. Considering the different weights, sensitivity analysis helps understand the impact of changes in the problem's parameters on the solution.
3. Development of a building emulator with physic-based asset modeling to represent the system characteristics and operations for validation of the optimal sizing and dispatch solutions.

The remaining part of the paper is organized as follows: Section 2 describes the building energy asset modeling with the energy flow; Section 3 presents the optimization methods to solve the sizing and dispatch problem of thermal and battery storage in the building and describes the objective functions; Section 4 explains the building emulator to validate the optimal dispatch and co-simulation setup with optimization procedure; Section 5 describes the case study conditions to test the proposed methods; Section 6 shows the case study results, followed by the conclusions and discussion described in Section 7.

2. Building energy asset modeling

This section elaborates the thermal and battery storage models, along with the essential building energy assets, such as the HVAC (heating, ventilation, and air-conditioning) plant system, required to meet the building's thermal and electric demands for the optimal sizing and dispatch of this study. As the thermal storage operations are integrated with the HVAC plant system, it is required to model the systems taking into account operational characteristics and efficiency, for optimizing the sizing and dispatch of the overall system. The primary focus of this paper is on the cooling mode, where the chiller model operates for both charging the thermal storage and providing cooling. Fig. 1 shows the energy flow of the building energy systems with the thermal storage and battery. The ice storage model is used as thermal storage for cooling purposes. It is important to note that depending on the building types and operational requirements, alternative systems can be employed. For example, a heat pump can serve as an alternative to the chiller, and a boiler can be utilized for heating purposes with hot water thermal storage.

2.1. Thermal energy storage

In this work, the thermal energy storage (TES) dynamics are modeled considering the system capacity, temperature, mass flow rate of the loop, and demand. Based on the charging and discharging rates in the TES dynamics, the state of charge (SOC) level is estimated and leveraged to show the potential utilization of thermal energy storage, as in (1)–(8).

$$\epsilon_c(l^t_{\text{tes}}) = a_0 + a_1 l^t_{\text{tes}} + a_2 (l^t_{\text{tes}})^2 \tag{1}$$

$$\epsilon_d(l^t_{\text{tes}}) = b_0 + b_1 l^t_{\text{tes}} + b_2 (l^t_{\text{tes}})^2 \tag{2}$$

$$\bar{q}_{\text{ch}}(l^t_{\text{tes}}) = \epsilon_c(l^t_{\text{tes}}) \dot{m} c_p (T_{\text{fr}} - T_{\text{cw-ch}}) \tag{3}$$

$$\underline{q}_{\text{dis}}(l^t_{\text{tes}}) = \epsilon_d(l^t_{\text{tes}}) \dot{m} c_p (T_{\text{cw-norm}} - T_{\text{fr}}) \tag{4}$$

$$0 \le q^t_{\text{tes-ch}} \le \min\left(C_{\text{chiller}}, \left(\overline{L_{\text{tes}}} - l^{t-1}_{\text{tes}}\right) Q_{\text{tes}}, \bar{q}_{\text{ch}}(l^t_{\text{tes}})\right) \tag{5}$$

$$0 \le q^t_{\text{tes-dis}} \le \min\left(q_{\text{cool}}, \left(l^{t-1}_{\text{tes}} - \underline{L_{\text{tes}}}\right) Q_{\text{tes}}, \underline{q}_{\text{dis}}(l^t_{\text{tes}})\right) \tag{6}$$

$$l^t = l^{t-1}_{\text{tes}} + \frac{q^t_{\text{tes-ch}} - q^t_{\text{tes-dis}}}{Q_{\text{tes}}} \tag{7}$$

$$\underline{L_{\text{tes}}} \le l^t_{\text{tes}} \le \overline{L_{\text{tes}}} \tag{8}$$

where l^t_{tes} is the SOC of thermal storage at t, $\epsilon_c(l^t_{\text{tes}})$ and $\epsilon_d(l^t_{\text{tes}})$ are the heat transfer effectiveness at l^t_{tes}, $\dot{m}$ is the maximum mass-flow rate, c_p is specific heat capacity, T_{fr} is the freezing temperature, $T_{\text{cw-ch}}$ is the chiller water output temperature for ice-storage charging, $T_{\text{cw-norm}}$ is the chilled water supply temperature from ice storage, C_{chiller} is the chiller capacity, Q_{tes} is the TES capacity, $\underline{L_{\text{tes}}}$ and $\overline{L_{\text{tes}}}$ are the minimum and maximum of SOC level.

The charging rate $q^t_{\text{tes-ch}}$ should be lower than the chiller capacity that provides the thermal energy to the storage. In addition, the charging rate is constrained by a specific maximum charging rate $\bar{q}_{\text{ch}}(l^t_{\text{tes}})$ estimated with the maximum mass flow rate of the system (e.g., pump), temperature differences, heat transfer effectiveness ($\epsilon_c(l_{\text{tes}})$), and more as in (1),(3),(5). Similarly, the discharging rate $q^t_{\text{tes-dis}}$ should be lower than the required building cooling demand q_{cool} and a specific maximum discharging rate $\underline{q}_{\text{dis}}(l^t_{\text{tes}})$ as in (2),(4),(6). Both TES charging and discharging rates should also be limited by the SOC level constraints as in (7)–(8).

The TES tank volume V_{tes} can be calculated with the thermal capacity Q_{tes} [5] assuming the unit of Q_{tes} is Wh and it should fit in the space as (9).

$$V_{\text{tes}} = \frac{Q_{\text{tes}} \cdot 3600(\text{J/Wh})}{c_p \cdot \Delta T \cdot 1000(\text{kg/m}^3) \cdot \eta_{\text{tes}}} \le A_{\text{tes}} \cdot H_{\text{tes}} \tag{9}$$

where ΔT is the temperature difference, η_{tes} is the storage efficiency, H_{tes} is the height of the space, and A_{tes} is the floor area allocated to TES.

2.2. Electric chiller

The electric chiller model is developed with the functions of temperature and part load ratio (PLR) [25]. The power consumption of the chiller P_{chiller} is calculated for the chiller compressor, as in (10)–(15).

$$\psi_1(T_{\text{cw-s}}, T_{\text{cond-e}}) = a_0 + a_1 T_{\text{cw-s}} + a_2 T^2_{\text{cw-s}} + a_3 T_{\text{cond-e}} + a_4 T^2_{\text{cond-e}} + a_5 T_{\text{cw-s}} T_{\text{cond-e}} \tag{10}$$

$$Q_{\text{chiller-a}} = C_{\text{chiller}} \psi_1 \tag{11}$$

$$PLR = q_{\text{load}} / Q_{\text{chiller-a}} \tag{12}$$

$$\psi_2(T_{\text{cw-s}}, T_{\text{cond-e}}) = b_0 + b_1 T_{\text{cw-s}} + b_2 T^2_{\text{cw-s}} + b_3 T_{\text{cond-e}} + b_4 T^2_{\text{cond-e}} + b_5 T_{\text{cw-s}} T_{\text{cond-e}} \tag{13}$$

$$\psi_3(PLR) = c_0 + c_1 PLR + c_2 PLR^2 \tag{14}$$

$$P_{\text{chiller}} = \frac{Q_{\text{chiller-a}} \psi_2 \psi_3}{COP_{\text{ref}}} \tag{15}$$

where ψ_1 is defined to estimate the chiller's available capacity $Q_{\text{chiller-a}}$ with the function of chilled water supply setpoint temperature $T_{\text{cw-s}}$ and condenser entering temperature $T_{\text{cond-e}}$, PLR is the ratio of the load q_{load} to its available capacity $Q_{\text{chiller-a}}$, ψ_2 is defined to adjust the ratio of energy to actual load with the function of temperature ($T_{\text{cw-s}}, T_{\text{cond-e}}$), ψ_3 is to adjust the ratio of energy input to actual load with the function

of PLR, P_{chiller} is estimated with the ratio of energy input to actual load, chiller's available capacity and reference coefficient of performance (COP_{ref}).

2.3. Battery

The battery energy storage (BES) dynamics are modeled with the charging $p^t_{\text{bes-ch}}$ and discharging rates $p^t_{\text{bes-dis}}$ considering the charging $\eta_{\text{bes-ch}}$ and discharging efficiency $\eta_{\text{bes-dis}}$. The SOC level of the battery is leveraged to represent the percentage of the stored energy to the battery capacity C_{bes}, as in (16)–(19).

$$l^t_{\text{bes}} = l^{t-1}_{\text{bes}} + \left(p^t_{\text{bes-ch}} \cdot \eta_{\text{bes-ch}} - p^t_{\text{bes-dis}}/\eta_{\text{bes-dis}}\right)/C_{\text{bes}} \tag{16}$$

$$\underline{L_{\text{bes}}} \le l^t_{\text{bes}} \le \overline{L_{\text{bes}}} \tag{17}$$

$$0 \le p^t_{\text{bes-ch}}, p^t_{\text{bes-dis}} \le \bar{P}_{\text{bes}} \tag{18}$$

$$P^t_{\text{bes}} = p^t_{\text{bes-ch}} - p^t_{\text{bes-dis}} \tag{19}$$

where l^t_{bes} is the SOC of battery at t, $\underline{L_{\text{bes}}}$ and $\overline{L_{\text{bes}}}$ are the minimum and maximum SOC level of battery, $\bar{P}_{\text{bes}}$ is the maximum power rates.

The battery volume V_{bes} can be calculated with the capacity C_{bes} and the battery's energy density and it should fit in the space allocated to the battery installation as (20).

$$V_{\text{bes}} = \frac{C_{\text{bes}}}{\rho_{\text{bes}}} \le A_{\text{bes}} \cdot H_{\text{bes}} \tag{20}$$

where A_{bes} is the floor area allocated to battery, ρ_{bes} is the energy density of the Li-ion battery, and H_{bes} is the height of the space.

2.4. Building loads

The total building electric load P_{total} is the sum of non-flexible load P_{non} (e.g., lighting, plug load, etc.) and flexible load that is changed by chiller power for TES charging and cooling and the battery power, as (21).

$$P_{\text{total}} = P_{\text{non}} + P_{\text{chiller}} + P_{\text{bes}} \tag{21}$$

3. Multi-objective optimization for sizing and dispatch

This section describes the optimization approach including the objective functions, optimization method, and detailed algorithm. The objective function that we used in our optimization engine includes operational costs, capital costs, and carbon emission costs.

Operational costs include two components: energy charges and demand charges. Calculating the energy charge involves TOU rate tariffs for energy consumption across different periods (e.g., peak, off-peak, and shoulder hours); while demand charges are based on the highest electric demand within a specified time interval, typically one month. The total operational cost can be mathematically expressed as (22):

$$C_{\text{op}} = \sum_{t=1}^{T} \lambda^t P^t_{\text{total}} + \sum_{m} \nu^m P^m_{\text{peak}} \tag{22}$$

where λ^t and ν^m denote the energy charge at time t given the length of the time horizon is T and the demand charge for month m, respectively. Additionally, P^m_{peak} denotes the peak demand within month m.

The annuity of the capital cost of the whole system can be represented by (23):

$$C_{\text{cap}} = \beta\left(\alpha_1 C_{\text{chiller}} + \alpha_2 Q_{\text{tes}} + \alpha_3 \bar{P}_{\text{bes}} + \alpha_4 C_{\text{bes}}\right) \tag{23}$$

where coefficients $\alpha_1, \cdots, \alpha_4$ represent the unit prices for the energy assets, and β denotes the capital recovery factor.

Finally, the emission cost represents the cost associated with the emissions resulting from the energy consumption. A general mathematical expression of the emission cost can be as (24):

$$C_{\text{em}} = \sum_{t=1}^{T} \left(c_{\text{carbon}} P^t_{\text{total}} MEF^t\right) \tag{24}$$

where MEF^t denotes the marginal emission factor varying by time t. c_{carbon} denotes the carbon value ($\$/kg$).

3.1. Optimal dispatch formulation

The optimal dispatch proposed in this work is to determine the charging/discharging rates of TES and BES, aiming to minimize the total operational cost, as well as the emission cost:

$$\min \quad C_{\text{op}} + w_k C_{\text{em}} \tag{25}$$

$$\text{subject to} \quad P^m_{\text{peak}} \ge P^t_{\text{total}}, \quad \forall t \in \{t \mid \text{month}(t) = m\} \tag{26}$$

$$\text{TES model (1)–(8), Chiller model (10)–(15)} \tag{27}$$

$$\text{BES model (16)–(19)} \tag{28}$$

where in the objective function (25) w_k denotes a nonnegative weight added to balance the emission cost for iteration in the algorithm 1. To decide the charging/discharging rates of TES and BES, the decision variables are $q^t_{\text{tes-ch}}, q^t_{\text{tes-dis}}, l^t, p^t_{\text{bes-ch}}, p^t_{\text{bes-dis}}, k^t, P^t_{\text{chiller}}, P^t_{\text{bes}}, P^t_{\text{total}}, P^m_{\text{peak}}$. Note that the optimal dispatch problem is to estimate the benefits with a given size of the whole system, where all energy asset sizes C_{chiller}, Q_{tes}, $\bar{P}_{\text{bes}}$, C_{bes} are treated as parameters. The capital cost is fixed and therefore is excluded from the optimization.

3.2. Optimal sizing formulation

The optimal dispatch formulation can be easily adapted to address sizing problems by including the system cost as a function of energy sizes in the objective function:

$$\min \quad C_{\text{op}} + C_{\text{cap}} + w_k C_{\text{em}} \tag{29}$$

$$\text{subject to} \quad P^m_{\text{peak}} \ge P^t_{\text{total}}, \quad \forall t \in \{t \mid \text{month}(t) = m\} \tag{30}$$

$$\text{TES model (1)–(9), Chiller model (10)–(15)} \tag{31}$$

$$\text{BES model (16)–(20)} \tag{32}$$

where the constraint set remains the same as the optimal dispatch problem except constraints (9), (20). These are to constrain the physical volume of the TES and BES in the optimal sizing problem. The optimal sizing aims to determine the size of the all energy assets (C_{chiller}, Q_{tes}, $\bar{P}_{\text{bes}}$, C_{bes}).

3.3. Multi-objective optimization method

In this work, multi-objective optimization deals with optimal sizing and dispatch problems considering conflicting objectives simultaneously. In the context of mixed-integer linear programming, both continuous and discrete decision variables are considered, and the objective function and constraints are formulated as linear relationships. The multi-objective optimization extends the single-objective case by having multiple objective functions, each representing a different goal. These objectives are usually conflicting, meaning that improving one objective might worsen another.

The weighted-sum method is chosen for practical and effective solutions of multi-objective optimization problems due to its computational efficiency, simplicity, and flexibility in objective trade-offs with decision-making processes. This approach allows for rapid exploration of the solution space. Furthermore, we can explore trade-offs between competing objectives by adjusting the weights assigned to each objective, making the process more intuitive and interpretable. This flexibility enables stakeholders to prioritize objectives according to their preferences and constraints, leading to tailored solutions that align with specific project goals and requirements.

The weighted-sum method provides a way to combine multiple objective functions into a single objective function. Our work adapted the weighted-sum method in solving the multi-objective problem in two stages as follows.

In Stage 1, we solve the multi-objective optimal sizing problem for the building energy storage system with the given weight value using the weighted-sum method. In Stage 2, the optimal dispatch problem is solved with the optimal sizing results from Stage 1. The two-stage procedure iterates over all the given weights and generates a set of optimal solutions corresponding to each weight value, hence the Pareto front can be formulated.

The detailed algorithm is formulated in Algorithm 1.

Algorithm 1: Two-stage Weighted-sum Approach for Multi-Objective Optimization

```
Set the range of weight vectors for updating w_k ∈ {w_0, ..., w_K};
Initialize the weights w_0 ;
for k ← 0 to K by 1 do
    Stage 1: Solve the updated optimal sizing problem (25)–(28) with updated weights, obtain the optimal sizing result set τ_k = {τ_k^TES, τ_k^BES}
    Stage 2: Solve the optimal dispatch problem (29)–(32) with the optimal sizing parameters τ_k and weight w_k
    Evaluate the optimal dispatch results and objective functions given (w_k, τ_k).
    Update weights to w_{k+1}.
end
Return ῡ_k = (w_k, τ_k), where k = 0, 1, ..., K
```

3.4. SP-metric for Pareto front evaluation

The SP-metric (Sparsity metric) is used to evaluate the diversity of solutions on the Pareto front. It measures how evenly the solutions are distributed and how well they cover the extent of the Pareto front. We defined it as the standard deviation of the distances between consecutive solutions in the Pareto front as Eq. (33).

$$\Delta = \frac{d_f + d_l + \sum_{i=1}^{M-1} |d_i - \bar{d}|}{d_f + d_l} \tag{33}$$

where M is the number of solutions on the Pareto front, d_i is the Euclidean distance between consecutive solutions in the objective space, d_f is the Euclidean distance between the first solution and the second solution, d_l is the Euclidean distance between the last solution and the second-to-last solution, and $\bar{d}$ is the average of all d_i values.

The Spread value ranges from 0 to ∞. A Spread value of 0 indicates that all solutions are evenly distributed, which is the ideal scenario. A larger Spread value indicates that the solutions are not evenly distributed.

4. Cosimulation

4.1. Building emulator

Building emulators are developed to validate and test the prospective sizing options and operation for thermal and battery storage systems in buildings. It simulates the thermal behavior and energy dynamics of building thermal zones and associated equipment to assess the performance in a virtual environment.

This study leverages the DOE prototype large office building models [26] to showcase the efficacy of the proposed framework. These models are chosen specifically because they are widely known as significant energy consumers. The DOE prototype building models have versions in 16 different climate zones to reflect different loads due to the climate conditions in the models. It consists of 12 floors designated for occupancy, as well as a designated zone on each floor for a data center. The zones designated for occupancy are arranged in a perimeter-and-core configuration, with 4 perimeter zones surrounding a core zone, as seen in Fig. 2. The occupied zones are serviced by a multi-zone VAV system via a chilled water loop for cooling and a hot water loop for heating and reheat. The chilled water loop consists of two water-cooled chillers servicing chilled-water cooling coils in the air-handling unit (AHU). The hot water loop consists of a natural gas-fired boiler servicing hot-water heating coils in the AHU and the VAV terminals. The data center zones are serviced by water-source heat pumps that reject heat to a common water loop. The model assumes time-varying occupancy mainly between the hours of 9 AM and 6 PM on weekdays, with the lighting, ventilation setpoints and zone temperature setpoints varied accordingly. Similarly, the datacenter has a time-varying schedule, with the electrical energy consumption (and associated radiation to the thermal zone) cycling in 4-month periods.

Table 1
Annual peak and average demands in three climate locations.

		Boston, MA	San Diego, CA	El Paso, TX
Cooling demand (kW)	Peak	2778	1207	3106
	Average	389	181	652
Electric demand (kW)	Peak	3811	2470	4205
	Average	959	823	1252

Based on the prototype large office building model, we developed our building emulator using EnergyPlus, a detailed whole-building energy simulation tool. The chilled water loop is modified to place thermal storage to charge the ice storage tank and then extract energy from it to meet the cooling load, as shown in Fig. 3. The ice storage tank is coupled with one of the two chillers, dedicated to charging the ice tank, to store the thermal energy, while the other chiller is dedicated to meeting the cooling loads in the building. Automated control loops operate the HVAC system and the base chiller to meet cooling loads. TES control is exposed to the optimal controller via an FMU interface.

4.2. Cosimulation setup

To test the optimal dispatch, the simulation is coupled with an optimal controller implementing MPC in a co-simulation setup, with Python-developed TES and BES models and a building emulator based on EnergyPlus, as illustrated in Fig. 4. The controller uses anticipated load, weather data, and measurements from the building model at each timestep to determine the optimal control action (described in Section 3). The Python-developed TES and BES models receive the charge or discharge rates from the optimal dispatch algorithm that is based on the current SOC. As for TES, the maximum possible charge/discharge rate is determined by given measurements from the chilled water loop and is compared with the rate requested by the controller. The lower of those two values is then passed on to the EnergyPlus model packaged as an FMU, with an interface exposed using the `ExternalInterface:FunctionalMockupUnitExport:To:Schedule` class. The EnergyPlus model has Energy Management System (EMS) class objects that automate the required actions based on the requested rate. These programs operate the chilled water loop components, including the chiller, chilled water pumps, heat exchangers, and thermal energy storage to achieve the requested charge/discharge rate. The simulation model progresses through each timestep, as measurements are obtained and subsequently sent to the controller. This iterative process continues as a continuous loop.

5. Case study conditions

The proposed multi-objective optimal sizing and dispatch is applied to the large office building models to assess the potential benefits of building energy storage systems depending on the climate location, utility rate tariffs (e.g., time-of-use (TOU), demand charge), and emission factors. Three locations are selected based on climate zones: Boston, MA, San Diego, CA, and El Paso, TX.

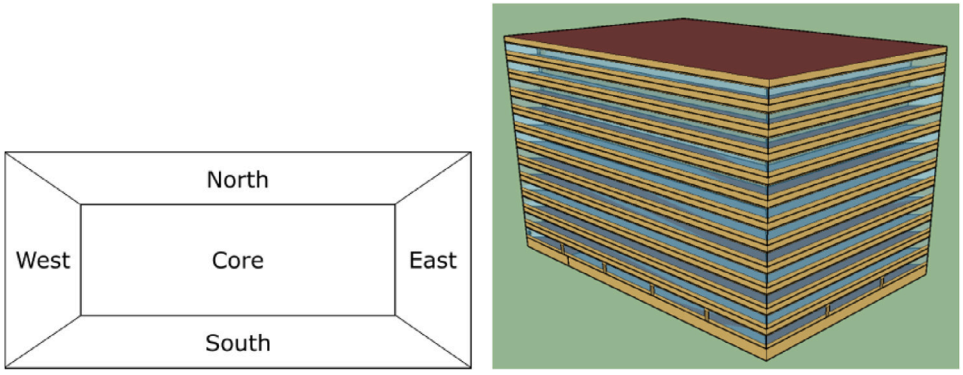

(a) Five-zone configuration (b) Building shape

Fig. 2. Zone configuration on each occupied floor and building shape of a large office prototype building model.

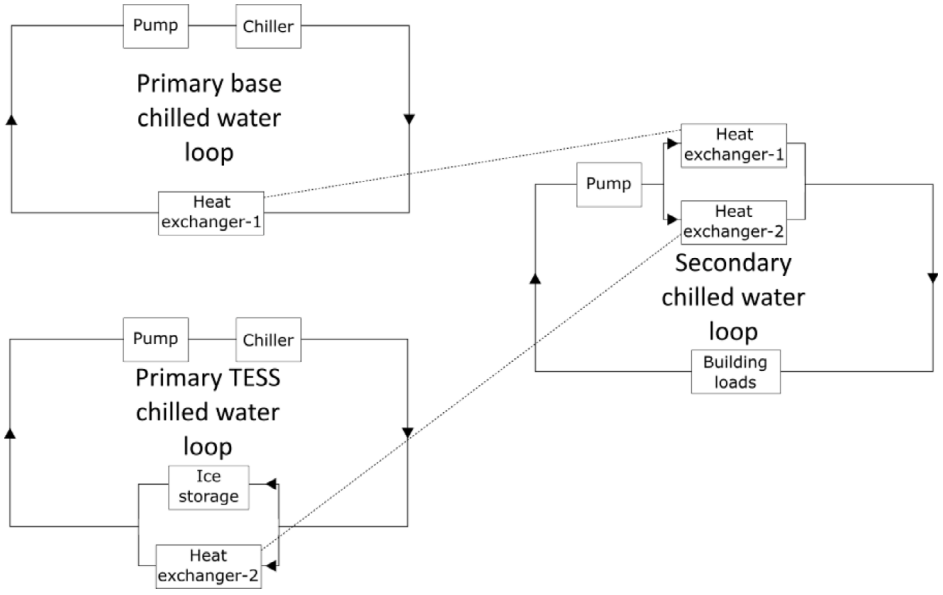

Fig. 3. Schematic of modified chilled water loop in EnergyPlus.

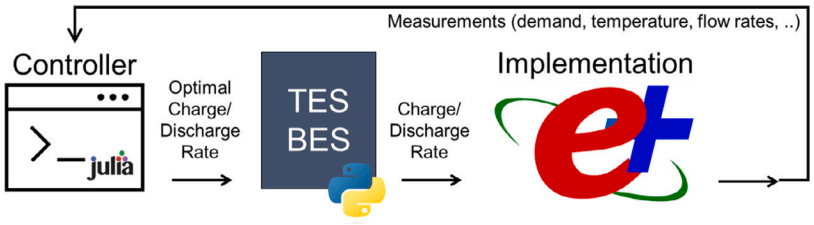

Fig. 4. MPC-based controller validation.

Table 1 provides the annual peak and average of the electric and cooling demands of the office building models in three different climate locations. As observed in the table, the peak and average cooling demands vary depending on the climate locations. The highest cooling demand is observed in El Paso with its hot summers, while the lowest cooling demand is shown in San Diego with its mild temperatures throughout the year. The average cooling demand is around 14%–21% of the peak demand. Considering the cooling systems are generally sized with the peak demand, the systems will run at their low part load ratio for most of the time and it will lead to inefficient operations. Fig. 5 further illustrates the duration curve of the cooling demand for each location. It is observed that the peak cooling demands occur a very small percentage of the time. As the load factor is significantly low, there are many opportunities to manage the peak demand more effectively. The electric demands also vary by the climate locations reflecting the HVAC electric demand to support the cooling and heating demand. The average electric demand is around 25%–33% of its peak demand. With this load analysis, we expect integrating the thermal and battery storage can help downsize the plant system. This will also contribute to smoothing out peaks by storing excess energy during non-peak periods and discharging it during peak demand periods.

Based on the hourly data, Fig. 6 illustrates monthly average electric and cooling demands for seasonal variations in different climate locations. As observed in Table 1, the cooling demands show larger variations compared to the electric demands. Particularly, El Paso shows the highest cooling demand with the largest variation ranging

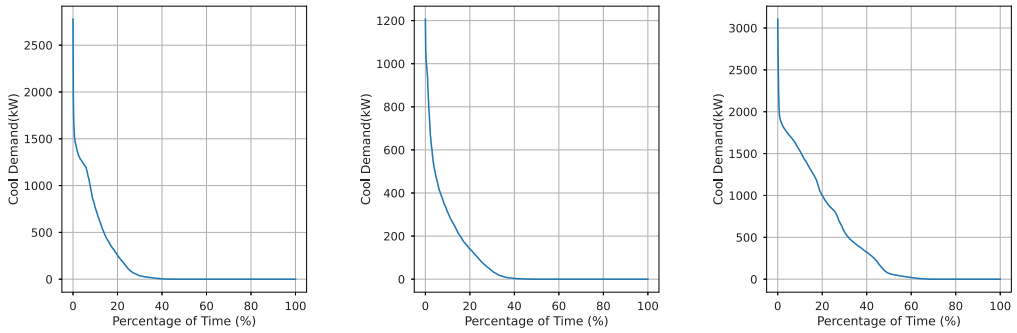

(a) Boston, MA (b) San Diego, CA (c) El Paso, TX

Fig. 5. Duration curve with cooling demand.

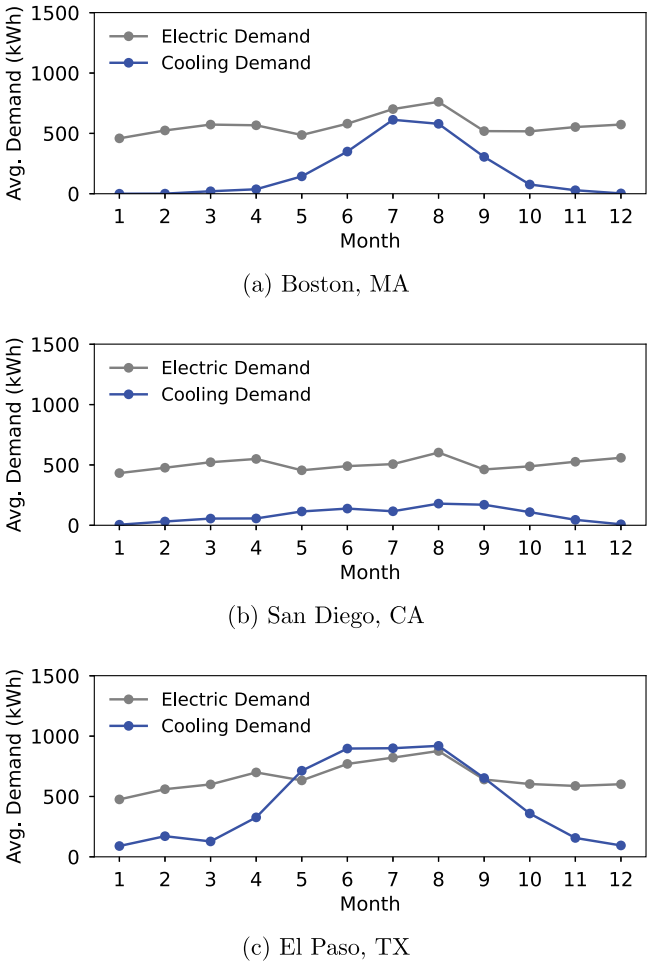

(a) Boston, MA

(b) San Diego, CA

(c) El Paso, TX

Fig. 6. Monthly average electric and cooling demands in three climate locations.

Table 2
Utility rate tariffs during June-September in different climate locations.

		Boston, MA	San Diego, CA	El Paso, TX
Demand charge ($/kW)		19	11.45	9.79
TOU charge ($/kWh)	Peak	0.02145	0.46893	0.15675
	Part-peak	NA	0.24385	NA
	Off-peak	0.01935	0.19273	0.0152

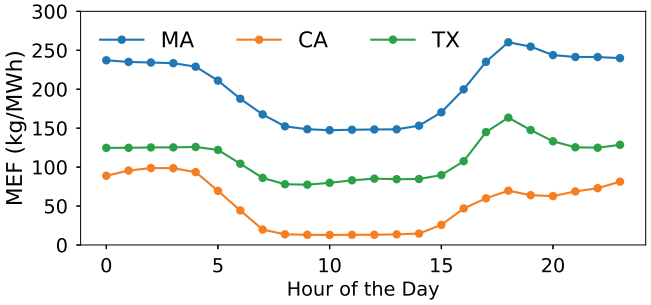

Fig. 7. Hourly marginal emission factor of a day for three locations.

from 90 to 920 kWh. El Paso has cooling demands even during the winter months. In contrast, Boston generally shows cooling demands during the summer months, ranging from 0 to 613 kWh. San Diego shows a relatively flat cooling demand throughout the year, ranging from 5 to 179 kWh. Unlike the cooling demand patterns, the electric demands show relatively smaller variations across both the time and location throughout the year. Note that the power consumption by the data center in the building model is excluded in this plot as it increases the power consumption level by 25% each month, and then reset every 4 months, as described in Section 4.1.

To identify the economic benefits of building energy storage, Table 2 summarizes the utility rate tariffs applied to the energy consumption for three locations, which are based on the United States Utility Rate Database [27]. The tariffs including demand charges and TOU charges may vary depending on the seasons and between weekends and weekdays. The presented table specifically outlines the applied utility rate tariffs during the months of June to September. The TOU charges vary based on the time of day, with different rates for peak, part-peak, and off-peak periods. In Boston, the TOU peak time is between 12 PM–7 PM. Although the gap between peak and off-peak rates is relatively low, the demand charge is the highest at $19/kW among the three locations. Meanwhile, San Diego has a highly dynamic TOU pricing structure with three distinct rates throughout the day. The peak rates occur during 4 PM–8 PM, which are approximately 4.8 times higher than the off-peak rates. El Paso has peak rates during 12 PM–5 PM and it shows the largest gap between the peak and off-peak rates, with an eightfold difference. Despite this, the demand charge is the lowest at $9.79/kW among the selected locations.

To consider the emission benefits of building energy storage, Fig. 7 illustrates the variation of the hourly marginal emission factor throughout the day generated from NREL's 2022 Cambium data sets [2]. Across all locations, the marginal emission factors are the lowest during daytime hours due to solar generation. These factors spike in the evening, as the sun goes down and conventional generators run to generate power. In the case of CA, the highest marginal emission factor occurs during the early morning hours. The marginal emission factor is

Table 3
Sizing parameters.

	Unit price	Max. capacity	Max. space
Chillers	$120/kW	10000 kW	
TES	$40/kWh	10000 kWh	500 m^2
BES	$355/kWh	10000 kWh	500 m^2
BES power	$153/kW	10000 kW	

the lowest in CA due to the extensive integration of renewable energy sources in electricity generation, while it is at its highest in MA. It is essential to note that these findings are derived from Cambium data and may not directly represent the actual emission rates of each location.

Additionally, we observe relationships between TOU pricing and MEF in these three locations. In CA, even though the MEF is the largest in the early morning, the MEF rise in the evening aligns with the peak TOU pricing (during 4–8 PM). In TX, as the MEF is low around 12 PM and spikes around 5 PM, it is not closely aligned throughout the entire peak TOU pricing period (12–5 PM). For MA, the MEF is at its lowest around 12 PM and spikes around 6 PM. Similar to TX, the TOU rate and MEF do not perfectly align during the peak TOU period (12–7 PM). While there is some correlation between TOU rates and MEF, particularly in the evening peak hours, the relationship is not consistent throughout the entire peak TOU pricing period across all locations. As the TOU pricing is designed to encourage customers to save electricity bills while MEF represents the emission factors associated with the electricity generation side, the TOU and MEF patterns are not perfectly aligned. However, combining two factors can allow customers to not only save electricity bills but also consider using electricity during periods with lower emissions.

The optimal sizing problem will cover a period of 20 years with a presumed discount rate of 5%. Table 3 outlines the unit price sourced from Energy Storage Cost and Performance Database [28] and physical constraints. The assumed efficiencies for both charging and discharging are set at 0.93, considering both battery and inverter. The case study aims to showcase the efficacy of a multi-objective optimal sizing and dispatch framework for forward-looking analysis and decision support. In this analysis, as for the baseline case, chiller capacities are determined based on the peak cooling demand without incorporating TES and BES.

6. Results

In this section, the multi-objective optimal sizing and dispatch of building energy systems with TES and BES will be explored. The framework based on Algorithm 1 is implemented in this case study for large office buildings located in three states under different TOU rates and marginal emission factors.

6.1. Multi-objective optimal sizing

6.1.1. Pareto-front solutions

We minimize the objective function (29) with economic ($C_{op}+C_{cap}$) and environmental (C_{em}) concerns to get the Pareto front optimal sizing solutions. As the weighted-sum method is applied to balance the two objectives, the analysis was performed using a diverse set of weight combinations to explore various trade-offs between the objectives.

The Pareto fronts for three locations, derived from a combination of 10 weight configurations with optimized sizing results, are illustrated in Fig. 8. To ensure a comprehensive exploration of the objective space, we selected weights ranging from 0 to 200. The initial weight is set to 0 to capture scenarios where one objective is entirely prioritized over the other. The last weight is set to 200 to observe the converse scenario. Intermediate weights were linearly distributed between 10 and 170 to build a 10-element weights collection: $w \in \{0, 10, 33, 56, 79, 101, 124, 147, 170, 200\}$. This selection and distribution of weights were based on preliminary analyses that suggested these values effectively delineate the trade-offs between objectives. By calibrating the weights in this manner, we ensured a detailed and representative mapping of the Pareto frontier, highlighting the distribution of optimal objective values. The blue lines in Fig. 8, representing Pareto fronts from optimal TES and BES sizes, identify a set of non-dominated, optimal solutions, demonstrating the trade-offs between minimizing economic objective (C_{op} + C_{cap}) and environmental objective (C_{em}). The representation confirms that the identified solutions lie on the Pareto frontier, highlighting their optimality in balancing the considered objectives.

Table 4
Pareto front sizing solution for Boston (MA)

#	w	$C_{op}+C_{cap}$ ($10^3$$)	C_{em} ($10^3$$)	Base chiller (kW)	TES chiller (kW)	TES (kWh)	BES Power (kW)	BES (kWh)
1	0	7,901	978	2300	300	4400	500	600
2	10	7,882	956	2300	300	4600	600	1000
3	33	8,021	949	2300	300	4400	700	1500
4	56	9,117	925	2300	300	3100	1000	3600
5	79	11,950	878	2300	300	2400	1000	8100
6	101	12,799	868	2300	300	3100	1000	9200
7	124	13,392	863	2300	300	3300	1000	10100
8	147	13,540	861	2300	300	3700	1000	10000
9	170	13,643	861	2300	300	4300	1000	10000
10	200	13,726	860	2300	300	4600	1000	10000

The Pareto fronts from three different locations all depicted a clear trade-off between minimizing economic objective (C_{op} + C_{cap}) and environmental objective (C_{em}). Solutions at one end of the Pareto front favored low emission costs, suitable for sustainability-focused strategies. Conversely, solutions at the other end prioritized cost-saving strategies but with marginally higher emission costs. Starting with zero weight value, the optimal solutions demonstrated a range of scenarios, from minimal cost-saving with acceptable emission levels to aggressive emission reduction with moderate cost increases. Notably, mid-range solutions provided a balanced approach, achieving significant reductions in both emission and total costs, which can be identified from Fig. 8, e.g., 4th solution in the middle of the blue lines.

The change of weights on each objective led to notable shifts in the Pareto front, reflecting the sensitivity of the optimization outcomes to the prioritization of objectives. The mid-range weights show a larger increase in C_{op} + C_{cap}, especially for the Boston case. With the same range of weights, between the 4th and 5th solution, the change of emission cost in the El Paso and San Diego cases are less than $30,000, while the emission cost decreases about $50,000. The $C_{op}+C_{cap}$ is more sensitive to the change of weights in all three locations. Given the same range of weight values, a higher weight on emission cost reduction shifted the Pareto front towards from $100,000 to $150,000 in three different cases, while the $C_{op}+C_{cap}$ can be shifted $6 million in Boston case, almost 40 times the emission cost changes.

Specific weight ranges, e.g., between the 3rd and 5th weights, $33 \le w \le 79$, revealed good balancing for the competing relationship between the two objectives. Beyond this range, the leftmost region leads to a more cost-saving strategy with less consideration of emission levels, while the rightmost region leads to a more aggressive emission reduction strategy and their corresponding optimal sizing and dispatching solutions.

Tables 4–6 and Fig. 9 summarize the Pareto front sizing solutions for each location. In Boston's case, the $C_{op}+C_{cap}$ (economic) is dominant in the sizing strategy where a larger TES capacity is prioritized over BES, resulting in a smaller BES. This is because of the small TOU rate gaps between peak and off-peak periods, making the investment in more expensive BES less economically advantageous compared to TES. With the TES, the base chiller's capacity could be reduced by 17.2% compared to the peak demand-based sizing. As we increase the significance of C_{em} (environmental consideration), the BES capacity rises,

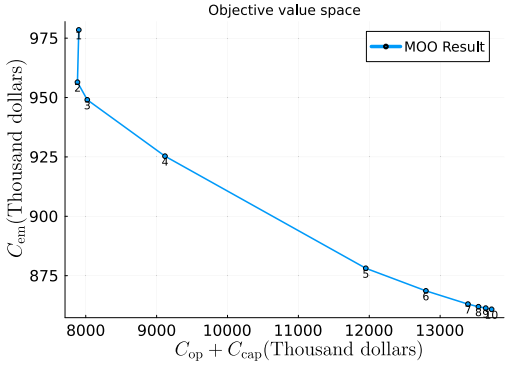

(a) Boston, MA

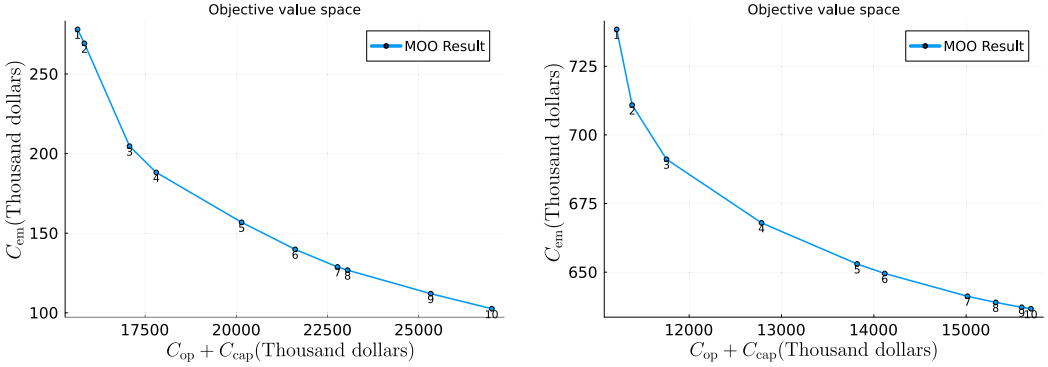

(b) San Diego, CA (c) El Paso, TX

Fig. 8. Pareto front of two objective functions with $K = 10$ iterations.

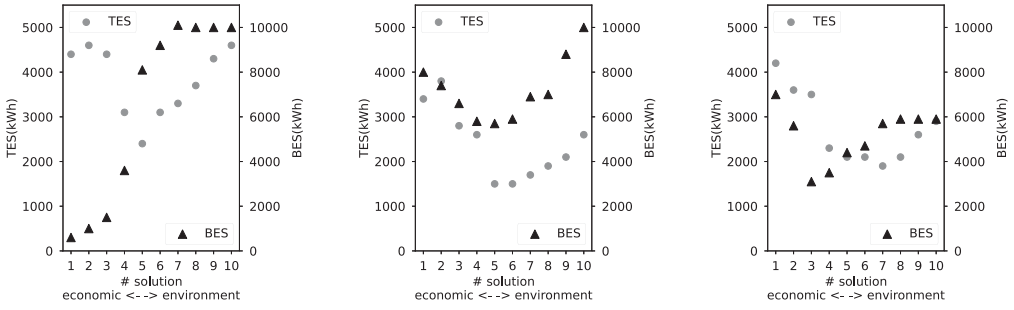

(a) Boston, MA (b) San Diego, CA (c) El Paso, TX

Fig. 9. Trends of TES and BES capacities.

Table 5
Pareto front sizing solution for San Diego (CA)

#	w	$C_{op} + C_{cap}$ ($10^3$$)	C_{em} ($10^3$$)	Base chiller (kW)	TES chiller (kW)	TES (kWh)	BES Power (kW)	BES (kWh)
1	0	15,649	278	900	200	3400	1000	8000
2	10	15,836	269	900	200	3800	1000	7400
3	33	17,074	204	900	200	2800	1000	6600
4	56	17,807	188	900	200	2600	1000	5800
5	79	20,145	156	1100	200	1500	1100	5700
6	101	21,614	139	1100	200	1500	1000	5900
7	124	22,774	128	1100	200	1700	1000	6900
8	147	23,050	126	1100	200	1900	1000	7000
9	170	25,329	112	1100	200	2100	1100	8800
10	200	27,005	102	1100	200	2600	1100	10 000

Table 6
Pareto front sizing solution for El Paso (TX)

#	w	$C_{op} + C_{cap}$ ($10^3$$)	C_{em} ($10^3$$)	Base chiller (kW)	TES chiller (kW)	TES (kWh)	BES Power (kW)	BES (kWh)
1	0	11,215	738	2700	200	4200	1000	7000
2	10	11,382	710	2700	200	3600	1000	5600
3	33	11,754	691	2700	200	3500	1100	3100
4	56	12,783	667	2700	200	2300	1100	3500
5	79	13,819	652	2700	200	2100	1000	4400
6	101	14,118	649	2700	200	2100	1000	4700
7	124	15,014	641	2700	200	1900	1000	5700
8	147	15,319	638	2700	200	2100	1100	5900
9	170	15,601	637	2700	200	2600	1000	5900
10	200	15,701	636	2700	200	2900	1100	5900

while the TES capacity reduces from 2nd to 4th solutions. The trend shifts when the C_{em} takes dominant, resulting in large capacities for both TES and BES, irrespective of their higher investment costs. Unlike the Boston case, when the $C_{op} + C_{cap}$ (economic) is dominant in the sizing strategy, investing in larger TES and BES is cost-effective for both San Diego and El Paso cases. As the focus shifts from purely economic benefits towards environmental concerns (C_{em}), the capacities of both TES and BES decrease from the second to the fifth solutions. However, starting from the sixth solution, capacities rise again. This shift indicates a strategy towards prioritizing larger TES and BES capacities to maximize environmental benefits rather than primarily emphasizing economic advantages. Leveraging TES utilization in San Diego and El Paso leads to a significant reduction in base chiller capacities ranging from 9%–25% and 13%, respectively.

Overall, it is important to note that when the economic considerations ($C_{op} + C_{cap}$) dominate the sizing strategy, the optimal sizing solutions are primarily determined by the utility tariffs specific to each location. Both San Diego and El Paso have large differences between the peak and off-peak TOU rates, making substantial energy storage investments economically viable. On the other hand, the Boston case is characterized by small differences between the peak and off-peak TOU rates, leading to the low economic viability of larger energy storage investments. When the environmental concerns (C_{em}) dominate the sizing strategy, larger TES and BES capacities are recommended to maximize environmental benefits. Please note that these optimal sizing solutions serve as guiding purposes. In practical applications, limited models are available from manufacturers, and commercial sizes should be selected considering real-world constraints and market offerings.

6.1.2. Evaluation of the Pareto-front solutions

We assessed the SP values of the Pareto-front solutions, utilizing data from Tables 4–6. The SP values for the cases in Boston (MA), San Diego (CA), and El Paso (TX) cases are 51.43, 3.91, and 11.88, respectively. Among the evaluated scenarios, the Boston case shows the least uniform distribution of solutions which means a potential clustering of solutions in specific regions of the Pareto front, while other areas remained sparse. The San Diego case has the most evenly distributed solutions among the three cases, with the SP value closest to the ideal scenario of having all solutions evenly distributed. The El Paso case has more evenly distributed solutions than the Boston case but there is still some variation in the distribution.

The analysis of the SP-metric highlights the variability in the distribution of Pareto-front solutions across different cases. However, it is important to note that the weight factor was fixed for all cases.

The relatively higher SP value in the Boston case indicates that adjusting the weight factors could enhance the robustness of its Pareto front to achieve a more uniform distribution. Introducing variable weight factors tailored to each case could address the unfairness caused by using a fixed weight factor. This would allow for a more customized approach that takes into account the unique aspects of each case. While the SP value for the Boston case is relatively higher, it does not necessarily indicate poor solutions. Instead, it signifies a need for potential adjustment in the weighting scheme to achieve a more balanced distribution of solutions. The Boston case solutions still represent valid trade-offs between economic and environmental objectives, but the result suggests that these solutions are more clustered, which can provide insight into specific areas where trade-offs are more pronounced.

6.2. Performance and benefit evaluation

Based on the Pareto front sizing, this section evaluated the optimal dispatch solutions and performed the energy, cost, and emission benefit analysis. Fig. 10 visualizes the electric load and SOC trends for both TES and BES across different solutions (#1, #4, #10, and baseline case) from July 1st to 8th in San Diego to provide a comparative analysis. The top subplot shows the load comparison, while the bottom subplots illustrate the SOC trends for each solution. Solution #1, primarily driven by economic consideration (C_{op}), charges both TES and BES during early morning hours and utilizes the stored energy during the day, to maximize the economic benefits from the TOU pricing structure. In addition, TES charging is prioritized over BES charging when the required electric demand is lower. On the other hand, Solution #10, which emphasized the environmental concerns (C_{em}), charges the TES and BES during the day when the emission factors are lower, even leading to a higher peak load compared to the baseline. Solution #4 balances the optimal dispatch between the economic and environmental concerns, charging energy in the morning and at night to leverage relatively lower emission and energy charge rates while avoiding peak hours.

Table 7
Comparison of the energy and costs under the optimal solutions and the baseline case in Boston.

	Baseline	#1	#4	#10
Total energy (MWh)	839 –	853 −1.7%	856 −2.0%	859 −2.4%
Emission ($)	7,854 –	7,983 −1.6%	7,862 −0.1%	7,794 0.8%
Energy charge ($)	16,920 –	17,191 −1.6%	17,220 −1.8%	17,257 −2.0%
Demand charge ($)	34,487 –	30,731 10.9%	32,446 5.9%	36,669 −6.3%
Total operation cost ($)	51,407 –	47,922 6.8%	49,666 3.4%	53,926 −4.9%

Table 8
Comparison of the energy and costs under the optimal solutions and the baseline case in San Diego.

	Baseline	#1	#4	#10
Total energy (MWh)	723 –	757 −4.7%	753 −4.1%	764 −5.7%
Emission ($)	1,596 –	2,175 −36.3%	1,579 1.1%	928 41.9%
Energy charge ($)	135,714 –	85,582 36.9%	101,966 24.9%	149,560 −10.2%
Demand charge ($)	18,390 –	18,247 0.8%	22,746 −23.7%	28,334 −54.1%
Total operation cost ($)	154,104 –	103,829 32.6%	124,712 19.1%	177,894 −15.4%

Fig. 11 presents the energy charge and emission costs for the different solutions (#1, #4, #10, and baseline case) from July 1st to 8th in San Diego. As observed in the optimal dispatch patterns, Solution #1 showed high emission costs by charging during early morning hours with relatively high emission factors. However, the energy charge was the lowest throughout the day among the other cases. Solution #10 showed significantly large energy costs during the day as it charges both TES and BES during the day when the emission factors are the lowest. Solution #4 tries to find a balance between Solution #1 and #10. Thus, there are low energy charges during the peak hours, and although it shows higher emissions at night by charging the energy, the charging duration is short enough to keep overall emissions relatively low compared to Solution #1.

We conducted a comprehensive performance analysis of optimal dispatch strategies over a one-month operation during the summer, comparing a baseline approach with a multi-objective solution to assess their impact on energy, economic, and environmental factors. The results are presented in Tables 7–9, highlighting the total energy consumption, peak load, energy charge, demand charge, and emission costs in August. In the Boston case, we observe 1.7–2.4% more energy consumption with the optimal solutions compared to the baseline, which has no energy storage system. As its utility rate tariffs are characterized

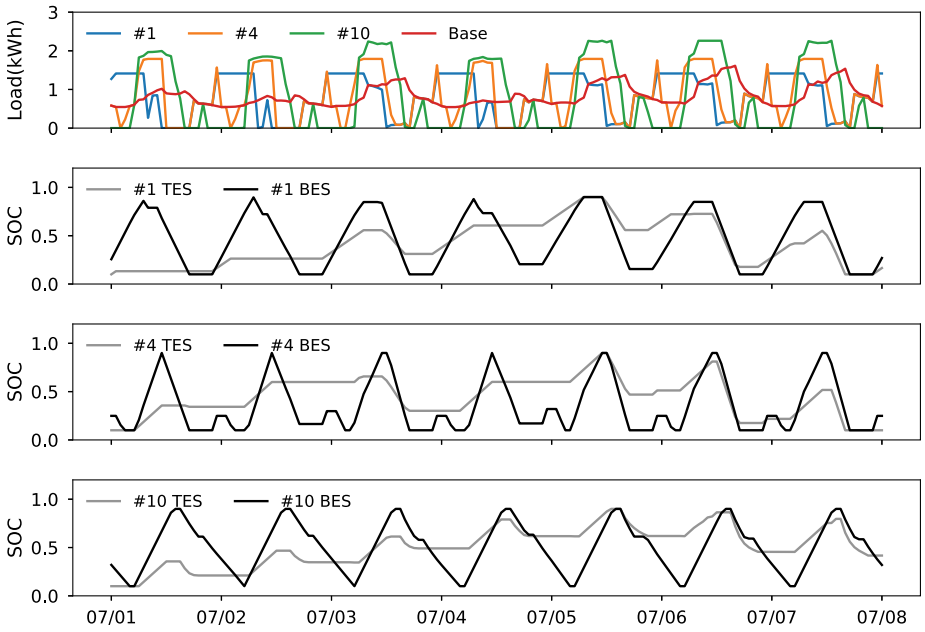

Fig. 10. The electric load and State of Charge of TES and BES for Solution #1, #4, #10, and the baseline case in San Diego.

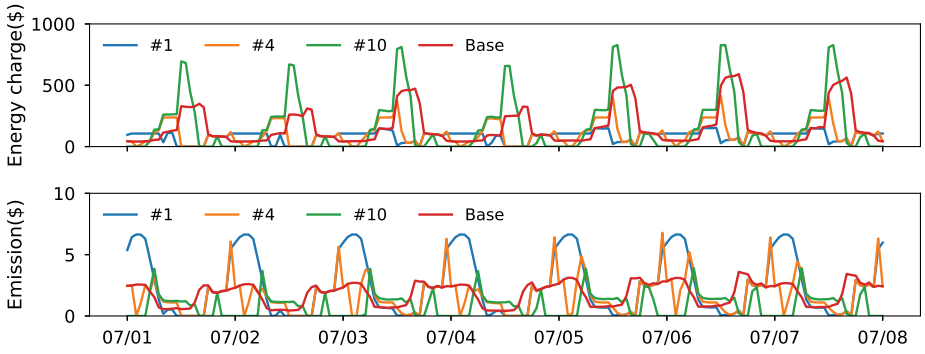

Fig. 11. The energy charge and emission costs for Solution #1, #4, #10, and the baseline case in San Diego.

Table 9
Comparison of the energy and costs under the optimal solutions and the baseline case in El Paso.

	Baseline	#1	#4	#10
Total energy (MWh)	920 –	969 −5.3%	959 −4.2%	951 −3.4%
Emission ($)	4,731 –	5,132 −8.5%	4,574 3.3%	4,588 3.0%
Energy charge ($)	53,863 –	30,803 42.8%	44,742 16.9%	51,046 5.2%
Demand charge ($)	18,840 –	17,691 6.1%	25,009 −32.7%	22,774 −20.7%
Total operation cost ($)	72,703 –	48,494 33.3%	69,751 4.1%	73,820 −1.5%

by a small difference between peak and non-peak TOU energy charges, it does not show economical benefits in terms of energy charge with energy storage system utilization. With a high demand charge, Solution 1, which prioritized economical benefits the most, demonstrates a 10.9% demand charge saving due to peak load reduction and a 6.8% total operation cost saving while 1.6% higher emission than the baseline. Solution 10, which prioritized environmental concerns the most, shows emission savings at 0.8% compared to the baseline but has a total operation cost 4.9% higher than the baseline. The relatively low environmental benefit is due to its MEF difference between the lowest and highest is around 1.8 times. It is observed that the difference is not sufficient to generate larger environmental benefits by utilizing the building energy storage systems. Solution 4 balances economic and environmental concerns well in its dispatch strategy so that it achieves a 3.4% operation cost saving with only a 0.1% increase in emissions. In the San Diego case, the optimal solutions lead to an increase of 4.1–5.7% in total energy consumption. Due to its relatively larger gap between the TOU non-peak and peak pricing structure, Solution 1, which dominates the economic concerns, shows a 36.9% energy charge saving and a corresponding 32.6% total energy cost saving. However, emissions are 36.3% higher than the baseline. In the San Diego case, the MEF difference between the lowest and highest values exceeds 7.7 times, thus the integration of environmental concerns into the strategy significantly influences the overall benefits. Solution 10 which prioritizes emission reduction, achieves a substantial 41.9% carbon emission decrease compared to the baseline, although it could not generate either energy or demand charge benefits. In the El Paso case, similar to the San Diego case, when the optimal solution prioritized the economic benefits, it achieved significant savings in total operation cost, up to 33.3%, with a slight increase in emissions by 8.5% compared to the baseline. Conversely, when the optimal solution concerns the environmental benefits more, the strategy results in a 3% emission reduction with a 1.5% higher total operation costs compared to the baseline. The solution considered both economic and environmental

Table 10
Computation Time per iteration for different locations.

Case name	Total time (min)	Sizing time (min)	Dispatch time (min)
Boston, MA	47	40	7
San Diego, CA	58	50	8
El Paso, TX	48	37	11

benefits could find a balance and demonstrate that the optimal strategy can save both emission and total operation costs.

In summary, all optimal solutions consume more energy compared to the baseline, as they leverage the building energy storage systems to achieve more economic or environmental benefits. Depending on the power pricing structure and the emission rates throughout the day, these solutions can get the benefit of both or either of these based on their prioritized concerns. Our analysis highlights the balanced trade-offs between economic gains, energy efficiency, and environmental impact across different locations.

6.3. Computation time

In this section, we delve into the computation time analysis for our multi-objective optimization framework applied to different geographical scenarios: Boston, San Diego, and El Paso. Each region presents unique energy profiles and environmental characteristics, influencing the complexity and computational requirements of the optimization process.

The analysis employed the same mixed-integer linear programming model across all cases, with region-specific data inputs such as TOU rates, emission factors, and energy demand profiles. The average computation time was calculated from the initiation to the completion of the optimization process for each iteration of the weights. The optimization engine runs on a MacOS 13.6 with 2.6 GHz 6-Core Intel Core i7 CPU and 16 GB RAM. The default software settings are Julia 1.6.3, JuMP v1.11, and HiGHS v1.5.2. For quality solution and computational efficiency, the HiGHS performed optimization with presolving, parallel computing, a specific relative gap for mixed-integer programming (MIP), and a maximum time limit for the solving process. The computation time results are shown in Table 10.

The computation time analysis across different geographical scenarios emphasizes the importance of considering regional energy profiles, regulatory environments, and demand patterns in the optimization of energy storage systems. We observed that the predominant factor contributing to time consumption across all cases was the resolution of the sizing problem, while the variation in weight values between iterations did not significantly impact the overall time. This understanding is crucial for developing efficient and regionally tailored energy management solutions.

7. Conclusion and discussion

To achieve economic and environmental synergy, this paper presented the multi-objective framework for optimal sizing and dispatch of building thermal and battery storage systems based on mixed integer linear programming and a weighted-sum approach. The proposed method addresses key challenges in optimal sizing, including operational efficiency oversights and conflicting objectives. Moreover, implementing a multi-objective optimization framework offers a comprehensive understanding of value streams, allowing decision-makers to balance conflicting goals effectively. As the framework adapts the weighted-sum approach, it is practical for decision-makers to explore various weight values and generate Pareto-front with economically viable and environment-friendly optimal solutions. Please note that this approach is introduced to find the dominant solutions on the Pareto-front, thus some points may be overlooked due to the non-convexity of the feasibility space, and they are considered non-dominated and isolated. For future work, we plan to refine the weighted-sum method with additional constraints for a more comprehensive exploration of the Pareto front.

The results demonstrated that the optimal building energy storage size varies with climate locations and prioritized objectives. It provides cost-effective sizing when the economic concerns are dominant, as the utility tariff with higher energy charge and demand charge significantly impacted the sizing of building energy storage systems, particularly BES, due to its higher capital costs. On the other hand, the substantial sizing for both TES and BES is determined when the environmental consideration is emphasized. Also, this proposed framework shows its capability for customers to not only save the electricity bills but also consider the emissions while using electricity.

Our work provides a foundation by generating initial optimal solutions promptly, enabling stakeholders to utilize them as a starting point for their final decision-making processes. Decision-makers should tailor the decision-making process to their specific context, taking into account additional factors as needed. They can utilize their preferred techniques, such as the TOPSIS or AHP method. Our approach ensures that decision-makers can explore and understand the value streams inherent in various objective streams.

While our method is developed and validated in specific contexts, demonstrating its effectiveness in diverse real-world scenarios will enhance confidence in its applicability. There are existing tools for battery storage analysis (e.g., ESET, DER-CAM, and QuEst); however, there is a lack of tools specifically for building thermal storage, making it difficult to compare our results in a real-world context. In future work, we plan to conduct more comprehensive validation studies across various building types, geographic regions, and operational settings and benchmark comparisons once more established and relevant benchmarks become available. It can support the generalizability of our method as well as enhance confidence in its applicability. This will also involve collaborating with industry partners and leveraging real-world data to assess the practical applicability of our method.

This research not only advances the theoretical understanding of building thermal and battery storage optimization but also offers practical methodologies for real-world implementation. As we continue to strive for sustainable and smart city development, our contributions support the affordable adoption of building energy storage for a more resilient and environmental urban landscape.

Considering the growing importance of electrification, our future work will explore how electrification impacts the integration of thermal and battery storage in buildings. For instance, how the intermittent nature of photovoltaic (PV) energy generation and dynamic electric vehicle (EV) loads can be incorporated into the overall building load to effectively use renewable energy resources and enhance the overall energy efficiency. Moreover, the proposed framework is scalable and flexible so that we can explore the potential benefits of building energy storage systems at the community level. This approach will provide a comprehensive understanding of energy dynamics in urban settings.

CRediT authorship contribution statement

Min Gyung Yu: Writing – original draft, Visualization, Validation, Software, Methodology, Conceptualization. **Bowen Huang:** Writing – original draft, Visualization, Validation, Software, Methodology, Conceptualization. **Xu Ma:** Writing – original draft, Validation, Software, Methodology, Conceptualization. **Karthik Devaprasad:** Writing – original draft, Validation, Software, Methodology, Conceptualization.

Declaration of competing interest

The authors declare that they have no known competing financial interests or personal relationships that could have appeared to influence the work reported in this paper.

Data availability

Data will be made available on request.

References

[1] Zurfi A, Albayati G, Zhang J. Economic feasibility of residential behind-the-meter battery energy storage under energy time-of-use and demand charge rates. In: 2017 IEEE 6th international conference on renewable energy research and applications. 2017, p. 842–9. http://dx.doi.org/10.1109/ICRERA.2017.8191179.

[2] Gagnon P, Cowiestoll B, Schwarz M. Cambium 2022 scenario descriptions and documentation. Tech. rep., 2023, URL https://www.nrel.gov/docs/fy23osti/84916.pdf.

[3] Electricity maps. 2023, https://app.electricitymaps.com/map. [Accessed 26 December 2023].

[4] Squalli J. Renewable energy, coal as a baseload power source, and greenhouse gas emissions: Evidence from U.S. state-level data. Energy 2017;127:479–88. http://dx.doi.org/10.1016/j.energy.2017.03.156, URL https://www.sciencedirect.com/science/article/pii/S0360544217305509.

[5] ASHRAE. 2000 HVAC systems and equipment. ASHRAE; 2007.

[6] Yik FWH, Lee WL, Burnett J, Jones P. Chiller plant sizing by cooling load simulation as a means to avoid oversized plant. HKIE Trans 1999;6(2):19–25. http://dx.doi.org/10.1080/1023697X.1999.10667801.

[7] Lee KH, Miedema AK. Modelling the potential of thermal storage for cooling under time-of-use electricity rates: An economic-engineering simulation approach. Int J Energy Res 1988;12(1):75–85.

[8] Henze GP, Biffar B, Kohn D, Becker MP. Optimal design and operation of a thermal storage system for a chilled water plant serving pharmaceutical buildings. Energy Build 2008;40(6):1004–19.

[9] Cui B, Gao D-c, Xiao F, Wang S. Model-based optimal design of active cool thermal energy storage for maximal life-cycle cost saving from demand management in commercial buildings. Appl Energy 2017;201:382–96.

[10] Lin W, Ma Z, McDowell C, Baghi Y, Banfield B. Optimal design of a thermal energy storage system using phase change materials for a net-zero energy solar decathlon house. Energy Build 2020;208:109626.

[11] He Z, Guo W, Zhang P. Performance prediction, optimal design and operational control of thermal energy storage using artificial intelligence methods. Renew Sustain Energy Rev 2022;156:111977.

[12] Wu D, Kintner-Meyer M, Yang T, Balducci P. Economic analysis and optimal sizing for behind-the-meter battery storage. In: 2016 IEEE power and energy society general meeting. 2016, p. 1–5. http://dx.doi.org/10.1109/PESGM.2016.7741210.

[13] Tsioumas E, Jabbour N, Koseoglou M, Papagiannis D, Mademlis C. Enhanced sizing methodology for the renewable energy sources and the battery storage system in a nearly zero energy building. IEEE Trans Power Electron 2021;36(9):10142–56. http://dx.doi.org/10.1109/TPEL.2021.3058395.

[14] Mehrtash M, Capitanescu F, Heiselberg PK, Gibon T, Bertrand A. An enhanced optimal PV and battery sizing model for zero energy buildings considering environmental impacts. IEEE Trans Ind Appl 2020;56(6):6846–56. http://dx.doi.org/10.1109/TIA.2020.3022742.

[15] Ikeda S, Ooka R. Metaheuristic optimization methods for a comprehensive operating schedule of battery, thermal energy storage, and heat source in a building energy system. Appl Energy 2015;151:192–205.

[16] Bilardo M, Ferrara M, Fabrizio E. Performance assessment and optimization of a solar cooling system to satisfy renewable energy ratio (RER) requirements in multi-family buildings. Renew Energy 2020;155:990–1008. http://dx.doi.org/10.1016/j.renene.2020.03.044.

[17] Baniasadi A, Habibi D, Al-Saedi W, Masoum MA, Das CK, Mousavi N. Optimal sizing design and operation of electrical and thermal energy storage systems in smart buildings. J Energy Storage 2020;28:101186. http://dx.doi.org/10.1016/j.est.2019.101186.

[18] Mehrtash M, Capitanescu F, Heiselberg PK. An efficient mixed-integer linear programming model for optimal sizing of battery energy storage in smart sustainable buildings. In: 2020 IEEE texas power and energy conference. 2020, p. 1–6. http://dx.doi.org/10.1109/TPEC48276.2020.9042498.

[19] Niu J, Tian Z, Lu Y, Zhao H. Flexible dispatch of a building energy system using building thermal storage and battery energy storage. Appl Energy 2019;243:274–87.

[20] Yu MG, Pavlak GS. Assessing the performance of uncertainty-aware transactive controls for building thermal energy storage systems. Appl Energy 2021;282:116103. http://dx.doi.org/10.1016/j.apenergy.2020.116103.

[21] Bre F, Lamberts R, Flores-Larsen S, Koenders EA. Multi-objective optimization of latent energy storage in buildings by using phase change materials with different melting temperatures. Appl Energy 2023;336:120806.

[22] Chen X, Liu Z, Wang P, Li B, Liu R, Zhang L, et al. Multi-objective optimization of battery capacity of grid-connected PV-BESS system in hybrid building energy sharing community considering time-of-use tariff. Appl Energy 2023;350:121727.

[23] Shah SK, Aye L, Rismanchi B. Multi-objective optimisation of a seasonal solar thermal energy storage system for space heating in cold climate. Appl Energy 2020;268:115047.

[24] Liu Z, Fan G, Sun D, Wu D, Guo J, Zhang S, et al. A novel distributed energy system combining hybrid energy storage and a multi-objective optimization method for nearly zero-energy communities and buildings. Energy 2022;239:122577.

[25] EnergyPlus engineering reference. 2023, EnergyPlus, https://energyplus.net/assets/nrel_custom/pdfs/pdfs_v23.2.0/EngineeringReference.pdf.

[26] Prototype building models. 2023, https://www.energycodes.gov/prototype-building-models.

[27] United States utility rate database. 2023, https://apps.openei.org/USURDB/.

[28] Energy storage cost and performance database. 2023, https://www.pnnl.gov/ESGC-cost-performance.